Colloid & Polymer Science Colloid Polym Sci 270:249–258 (1992)

The viscoelasticity of spinnable solutions of alkyltrimethylammonium salicylates

K. Hashimoto, T. Imae, and K. Nakazawa

Department of Chemistry, Faculty of Science, Nagoya University, Nagoya, Japan

Abstract: The viscoelasticity has been measured for aqueous solutions of tetradecyl- and hexadecyltrimethylammonium salicylates (C_{14}TASal, C_{16}TASal). The aqueous solutions of C_{14}TASal without salt displayed the gel-like behavior at 10.0×10^{-2} g cm^{-3}, but those more dilute than 3.2×10^{-2} g cm^{-3} presented the viscoelasticity similar to that of a Maxwell liquid. The Maxwell-like behavior was converted to the polymer-like one on the addition of (0.1–0.2) M NaBr or (0.02–0.2) M NaSal. The gel-like viscoelasticity can be connected with the spinnability of "cohesive fracture failure", and the Maxwell-like and polymer-like viscoelasticities are concerned with the spinnability of "ductile failure". The gel-like and Maxwell-like viscoelasticities originate in the pseudo-network formed by the pseudo-linkages between rodlike micelles, while the polymer-like viscoelasticity is caused by the entanglement of long rodlike micelles in semidilute and concentrated solutions. The aqueous solutions of C_{16}TASal behaved very similar to those of C_{14}TASal.

Key words: Viscoelasticity; spinnability; tetradecyltrimethylammonium salicylate; hexadecyltrimethylammonium salicylate; rodlike micelle

Introduction

Tetradecyldimethylammonium halides (C_{14}DAX) in water associate into long rodlike micelles on addition of salts such as sodium halides [1]. The semidilute solutions in which rodlike C_{14}DAX micelles entangle with each other exhibit non-Newtonian viscosity [2], but their viscoelasticity is not necessarily remarkable. Strong viscoelasticity is observed for aqueous solutions of cationic surfactants with aromatic counterions [3–12], which are also characterized by the spinnability [13].

We have recently measured spinnability and light scattering of aqueous solutions of tetradecyl- and hexadecyltrimethylammonium salicylates (C_{14}TASal, C_{16}TASal) [14–16]. The spinnability was classified into two types, ductile (D) type and cohesive fracture (C) type [17]. The light-scattering experiment elucidated that the pseudo-linkages between short rodlike micelles were formed in aqueous solutions with or without a small amount of sodium salicylate (NaSal), and the entanglement of long rodlike micelles existed in aqueous solutions with a medium amount of NaSal.

We investigate the viscoelasticity of aqueous solutions of C_nTASal (n = 14, 16) in this paper, and discuss the rheological properties of C_nTASal micelles in water.

Experimental section

The sample of C_{14}TASal was synthesized by mixing tetradecyltrimethylammonium chloride with NaSal in water, according to the previous method [14]. The crude crystals were recrystallized four times from water and twice from ethyl acetate. The samples of C_{16}TASal, ignited NaBr, and commercial NaSal are the same as previously prepared and used [14, 15]. Water was purified as usual.

The purity of the C_nTASal sample was certified by measuring surface tension γ in water as a function of surfactant concentration C(M); there was no minimum in the γ-log C plots for both surfactants, indicating the high purity of the sample. The critical micelle concentration (CMC), which is observed as the break point of the γ-log C curve, was 0.69 mM (0.025×10^{-2} g cm^{-3}) for C_{14}TASal and 0.10 mM (0.0042

$\times 10^{-2}$ g cm^{-3}) for C_{16}TASal at 25 °C. These were in agreement with the values in the literature, 0.625 and 0.15 mM, respectively [7], while they were lower than those of tetradecyl- and hexadecyltrimethylammonium bromides (C_{14}TAB, C_{16}TAB), 3.60 and 0.98 mM [18], respectively. The surface tension was constant above the CMC: 37.0, 30.4, 36.5, and 33.6 dyne cm^{-1} for C_{14}TASal, C_{16}TASal, C_{14}TAB, and C_{16}TAB, respectively.

The measurement of dynamic viscoelasticity was carried out on a Rheology Engineering MR-3 rheometer over frequencies of 0.005–3 Hz, by using Couette coaxial cylinder cells. The rheometer was set in an air bath, the temperature of which was controlled by circulating water. The temperature of solutions was kept within ± 1 °C.

Results

The absolute complex viscosity $|\eta^*|$, the storage modulus G', and the loss modulus G'', are shown in Fig. 1 as a function of angular frequency ω, for aqueous solutions of C_{14}TASal without salt at 25 °C. The $|\eta^*|$, G' and G'' values increased as the surfactant concentration increased. At surfactant concentrations below 3.2×10^{-2} g cm^{-3}, the $|\eta^*|$ values were constant at low frequencies, but decreased at higher frequencies. The G' values increased gradually with frequency, and the plateau was observed at higher frequencies. The G'' values increased gradually with the frequency and became constant at higher frequencies for a solution of 0.8×10^{-2} g cm^{-3}; G'' displayed a broad peak at $(1.2\text{–}3.2) \times 10^{-2}$ g cm^{-3}, similar to the viscoelasticity of a Maxwell liquid [19]. Aqueous solutions of 10.0×10^{-2} g cm^{-3} behaved differently: the $|\eta^*|$ decreased monotonically with the frequency and the G' and G'' were approximately constant over the whole frequency region examined, indicating the gel-like behavior [19].

Figures 2 and 3 show the $|\eta^*|$, G', and G'' plots at various NaBr and NaSal concentrations for aqueous solutions of C_{14}TASal of 1.6×10^{-2} g cm^{-3} (0.04 M) at 25 °C. As NaBr was added, the $|\eta^*|$ and G' decreased remarkably at lower frequencies, but increased slightly at higher frequencies. Therefore, at high NaBr concentrations, the constant region of $|\eta^*|$ widened to the higher frequency side and the plateau zone of G' shifted to the higher frequency region. The broad peak in the plot of log G'' vs log ω for an aqueous solution without salt sharpened and slightly shifted to the lower frequencies when 0.004 M NaBr was added, and the peak position shifted to the higher frequency side with further addition of NaBr. Above 0.1 M NaBr, the peak was not detected within the frequency range examined. The $|\eta^*|$, G' and G'' plots against ω were independent of NaBr concentrations above 0.1 M.

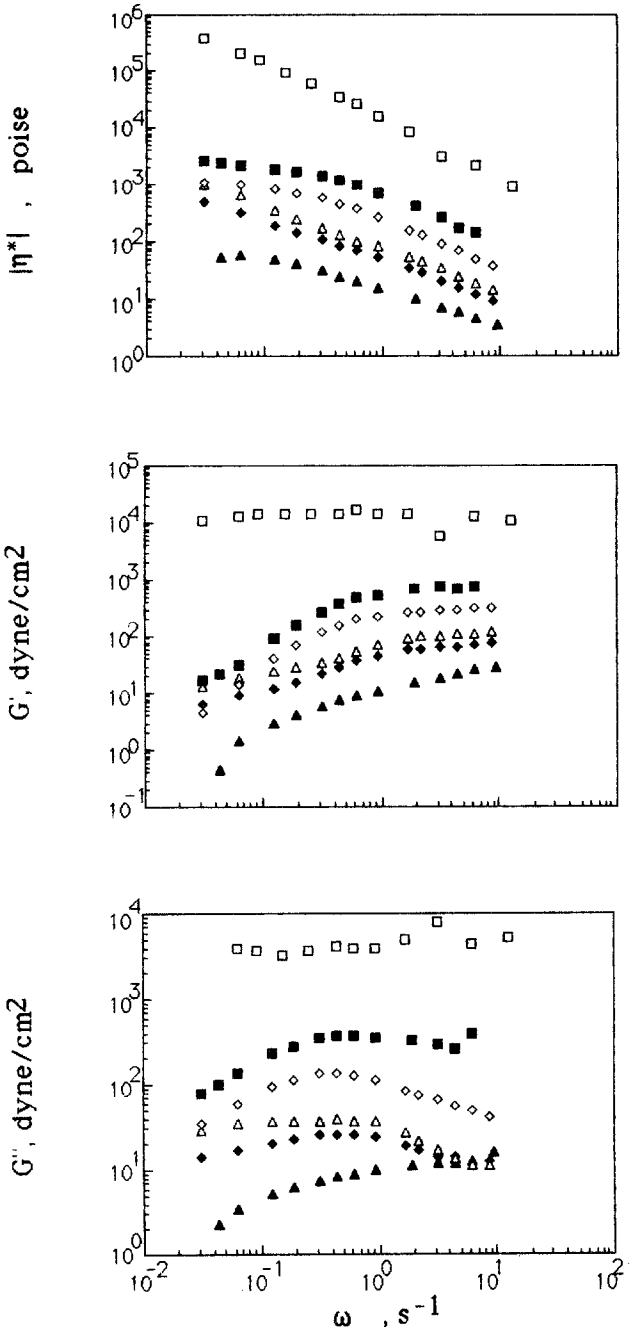

Fig. 1. The $|\eta^*|$, G', and G'' values as a function of angular frequency for aqueous solutions of C_{14}TASal without salt at 25 °C. c (10^{-2} g cm^{-3}): ▲) 0.8; ◆) 1.2; △) 1.6; ◇) 2.4; ■) 3.2; □) 10.0

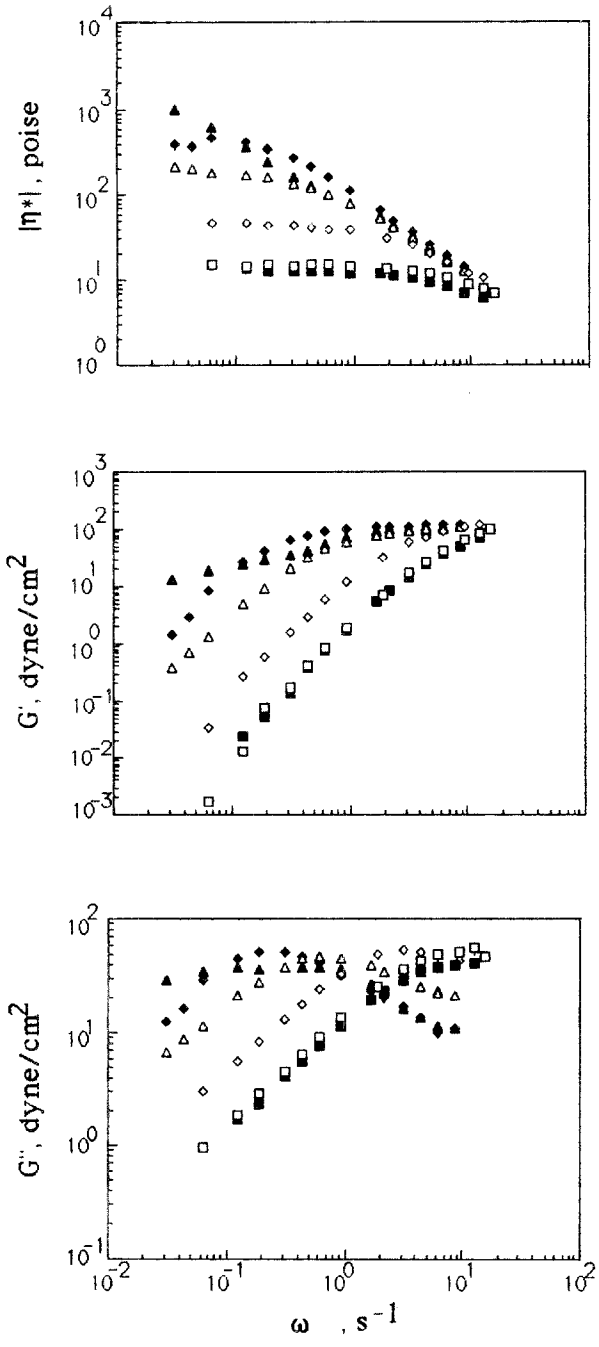

Fig. 2. The $|\eta^*|$, G', and G'' values as a function of angular frequency for aqueous NaBr solutions of $C_{14}TASal$ of 1.6 $\times 10^{-2}$ g cm^{-3} at 25 °C. C_s(M): ▲) 0; ◆) 0.004; △) 0.01; ◇) 0.04; ■) 0.1; □) 0.2

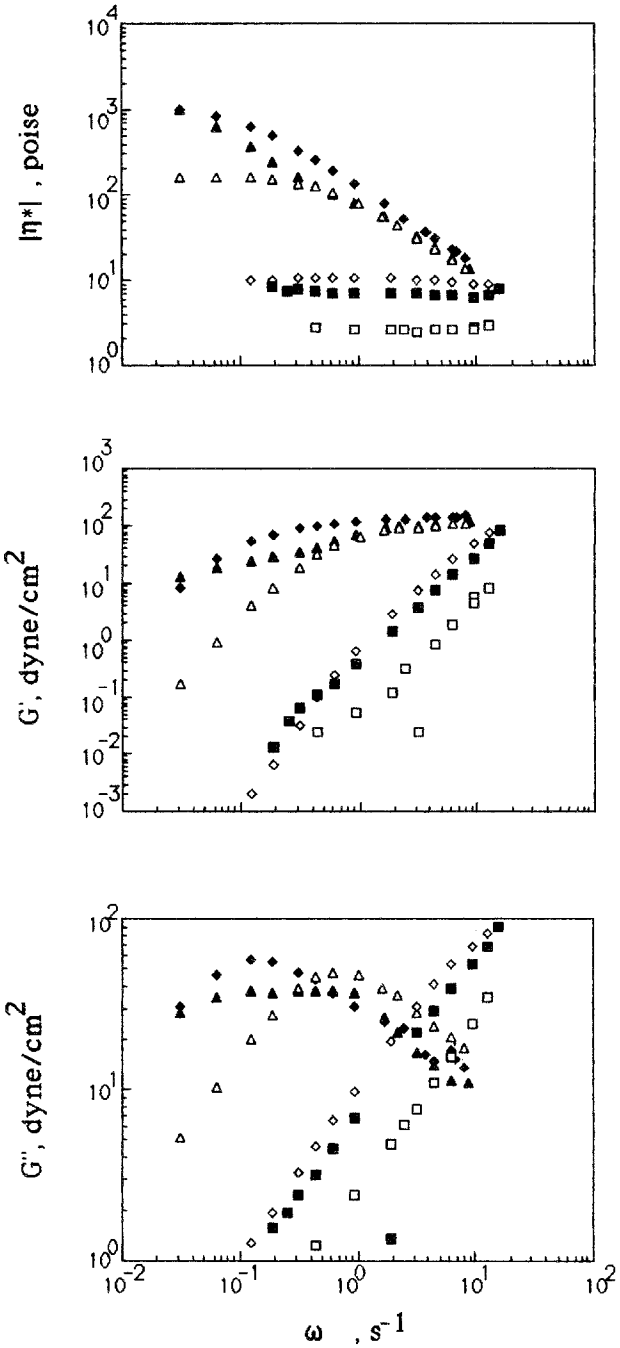

Fig. 3. The $|\eta^*|$, G', and G'' values as a function of angular frequency for aqueous NaSal solutions of $C_{14}TASal$ of 1.6 $\times 10^{-2}$ g cm^{-3} at 25 °C. C_s(M): ▲) 0; ◆) 0.001; △) 0.004; ◇) 0.02; ■) 0.1; □) 0.2

In the presence of 0.02 M NaSal, the $|\eta^*|$ values were independent of angular frequency, while the G' and G'' values increased almost linearly with frequency in a double logarithmic plot, suggesting the polymer-like behavior [19]. The salt effect occurred even at higher NaSal concentrations; the $|\eta^*|$, G' and G'' decreased with an increase in NaSal above 0.1 M, thus, differing with those in aqueous

NaBr solutions. They were too small to be measured with solutions of NaSal more concentrated than 0.5 M.

The temperature dependence of the $|\eta^*|$, G', and G'' values was examined for 0.2 M NaBr and NaSal solutions of C_{14}TASal of 1.6×10^{-2} g cm^{-3}, as represented in Figs. 4 and 5. The temperature rise from 15° to 35 °C reduced the $|\eta^*|$, G', and G'' values. The constant values of $|\eta^*|$ widened to the higher frequency side, and the plateau zone of G'

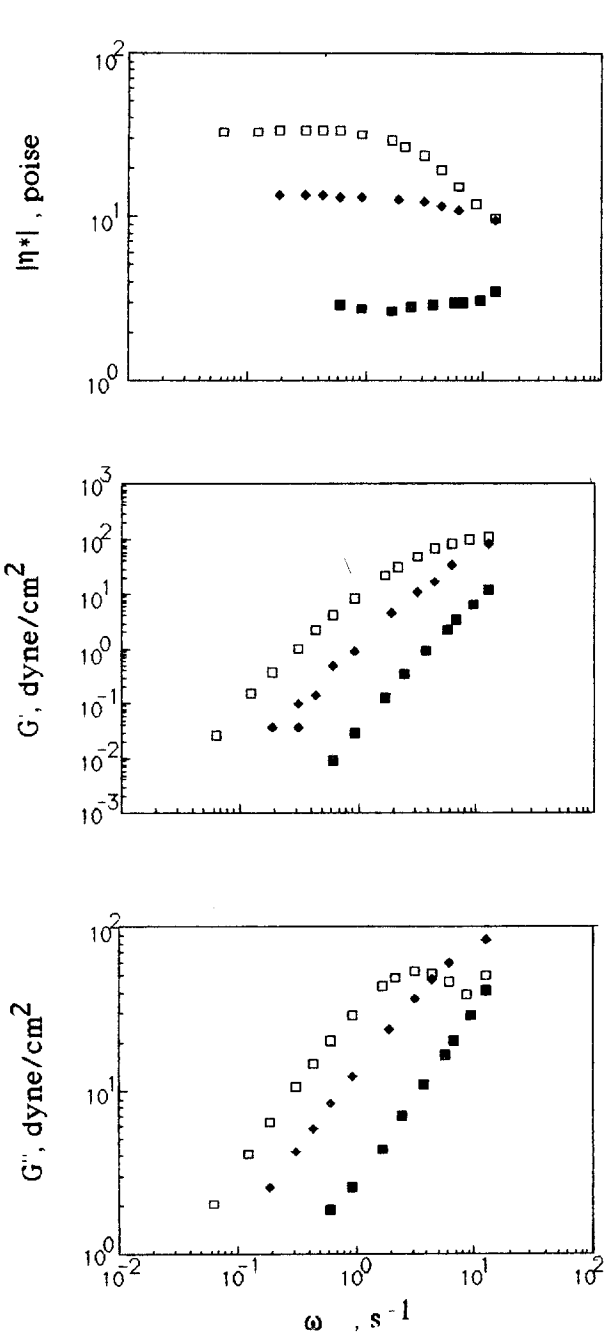

Fig. 4. The $|\eta^*|$, G', and G'' values as a function of angular frequency for 0.2 M NaBr solutions of C_{14}TASal of 1.6×10^{-2} g cm^{-3}. T(°C): □) 15; ◆) 25; ■) 35

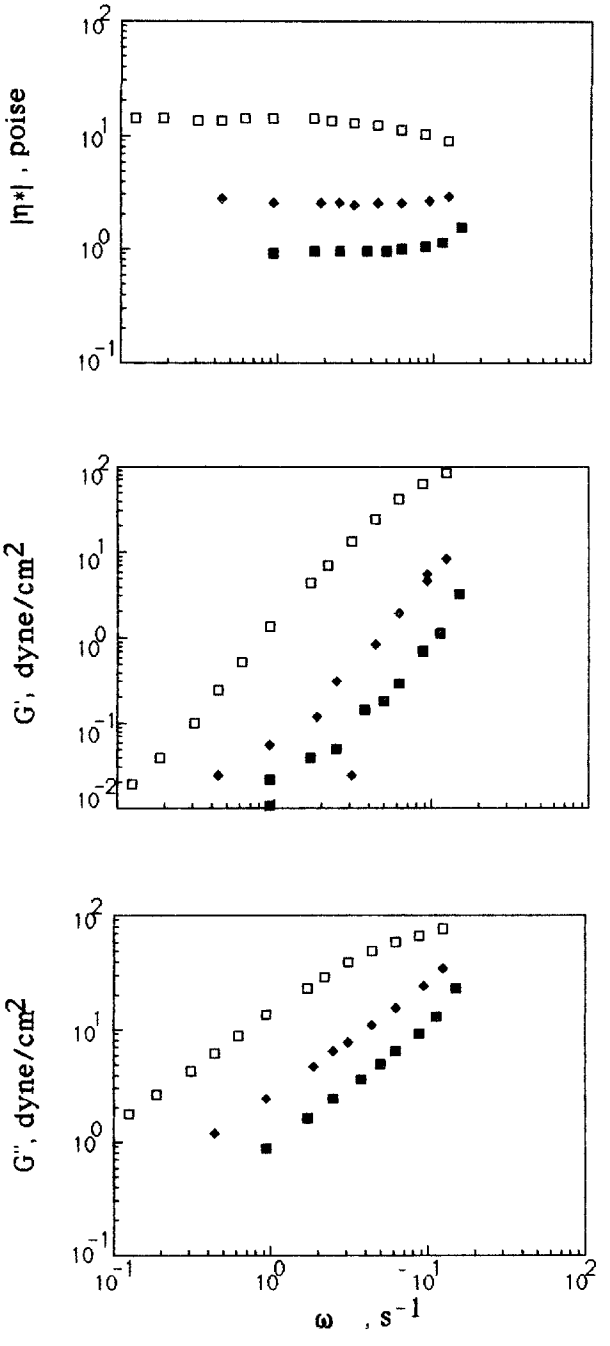

Fig. 5. The $|\eta^*|$, G', and G'' values as a function of angular frequency for 0.2 M NaSal solutions of C_{14}TASal of 1.6×10^{-2} g cm^{-3}. T(°C): □) 15; ◆) 25; ■) 35

and the maximum of G'' shifted to the higher frequency region, thus corresponding to the shift of relaxation toward higher frequencies or shorter times. Similar temperature dependence of $|\eta^*|$ and G' values as a function of angular frequency was observed for aqueous solutions of hexadecylpyridinium salicylate (C_{16}PySal) [6] and equimolar mixtures of C_{16}PySal + NaSal [9].

The viscosity at zero shear rate η_0 which can be obtained from the curves of $|\eta^*|$ against angular frequency [19, 20], is plotted in Figs. 6 and 7 as a function of surfactant or salt concentration, c ($g\,cm^{-3}$) or C_s(M), respectively. The η_0 values for aqueous solutions of C_{14}TASal without salt at 25 °C increased linearly with the surfactant concentration, and the slope was 3.20. The linear increase of the complex viscosity at $\omega = 0.01\ s^{-1}$ with surfactant concentration was reported for aqueous solutions of C_nTASal at 20 °C [6].

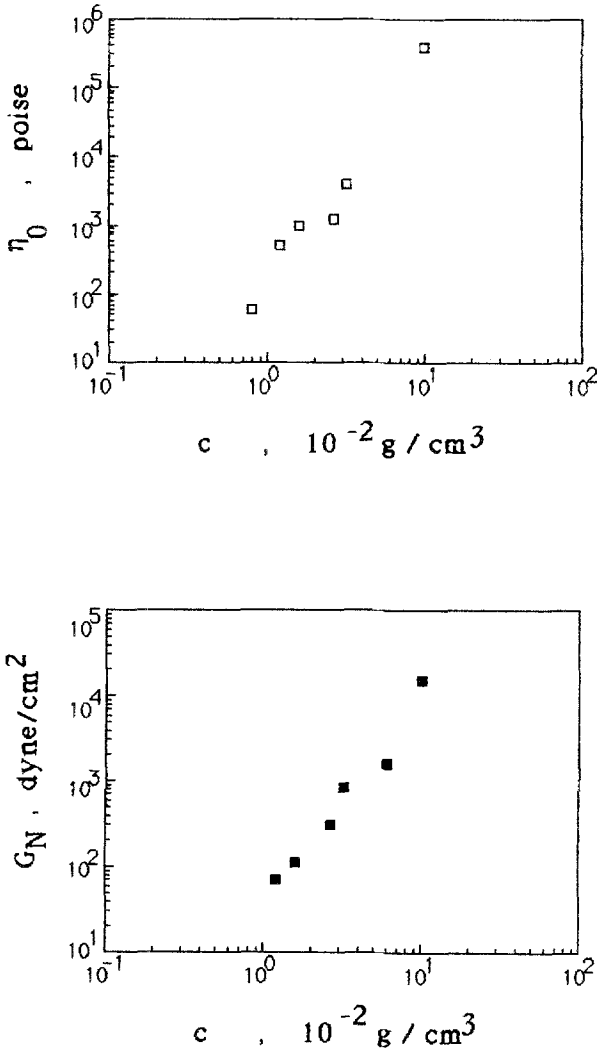

Fig. 6. The surfactant-concentration dependence of the η_0 and G_N values for aqueous solutions of C_{14}TASal without salt at 25°C

The η_0 values for aqueous NaBr solutions of C_{14}TASal decreased with an increase in NaBr concentration up to 0.1 M, but they were almost constant at 0.1–2 M NaBr. On the other hand, the η_0 values for aqueous NaSal solutions decreased through a large maximum at 0.0007 M and a small maximum at 0.1 M, as NaSal was added. Figure 7 includes the η_0 values for aqueous NaSal solutions of C_{16}TASal of $10^{-2}\ g\,cm^{-3}$ at 25 °C. There were two maxima at 0.003 and 0.1 M NaSal. It is obvious from Figs. 4 and 5 that the η_0 values for 0.2 M salt solution of C_{14}TASal of $1.6 \times 10^{-2}\ g\,cm^{-3}$ decrease as the temperature rises.

The dynamic modulus of the plateau G_N at high angular frequencies is plotted against surfactant and salt concentrations, respectively, in Figs. 6 and 7. The G_N values of aqueous solutions of C_{14}TASal without salt at 25 °C increased monotonically with increasing the surfactant concentration, as well as the zero shear viscosity. However, the G_N values, 110–120 dyne cm^{-2}, of aqueous salt solutions of C_{14}TASal of $1.6 \times 10^{-2}\ g\,cm^{-3}$ at 25 °C were independent of salt concentrations below 2 M NaBr or 0.01 M NaSal and salt species, NaBr or NaSal, despite that the zero shear viscosity depended on them.

The relaxation time which is the reciprocal of the angular frequency at the maximum in a G'' plot was 1.9–2.9 s for aqueous solutions of C_{14}TASal without salt at $(1.2–3.2) \times 10^{-2}\ g\,cm^{-3}$. Although the relaxation time increased with addition of 0.004 M NaBr or 0.001 M NaSal, it decreased with further addition of salts, indicating the variation of the relaxation mechanism with the salt concentration.

As seen in Figs. 1–5, the initial slope in a plot of log G' vs log ω was 0.41 for an aqueous solution of C_{14}TASal without salt at $1.6 \times 10^{-2}\ g\,cm^{-3}$, while that was about 2.0 for 0.001–0.2 M salt solutions. Although the gentle slope was obtained for aqueous solutions without salt at various surfactant concentrations, the slope of 2.0 was maintained at 15–35 °C for 0.2 M salt solutions at $1.6 \times 10^{-2}\ g\,cm^{-3}$. It can be noticed that the initial

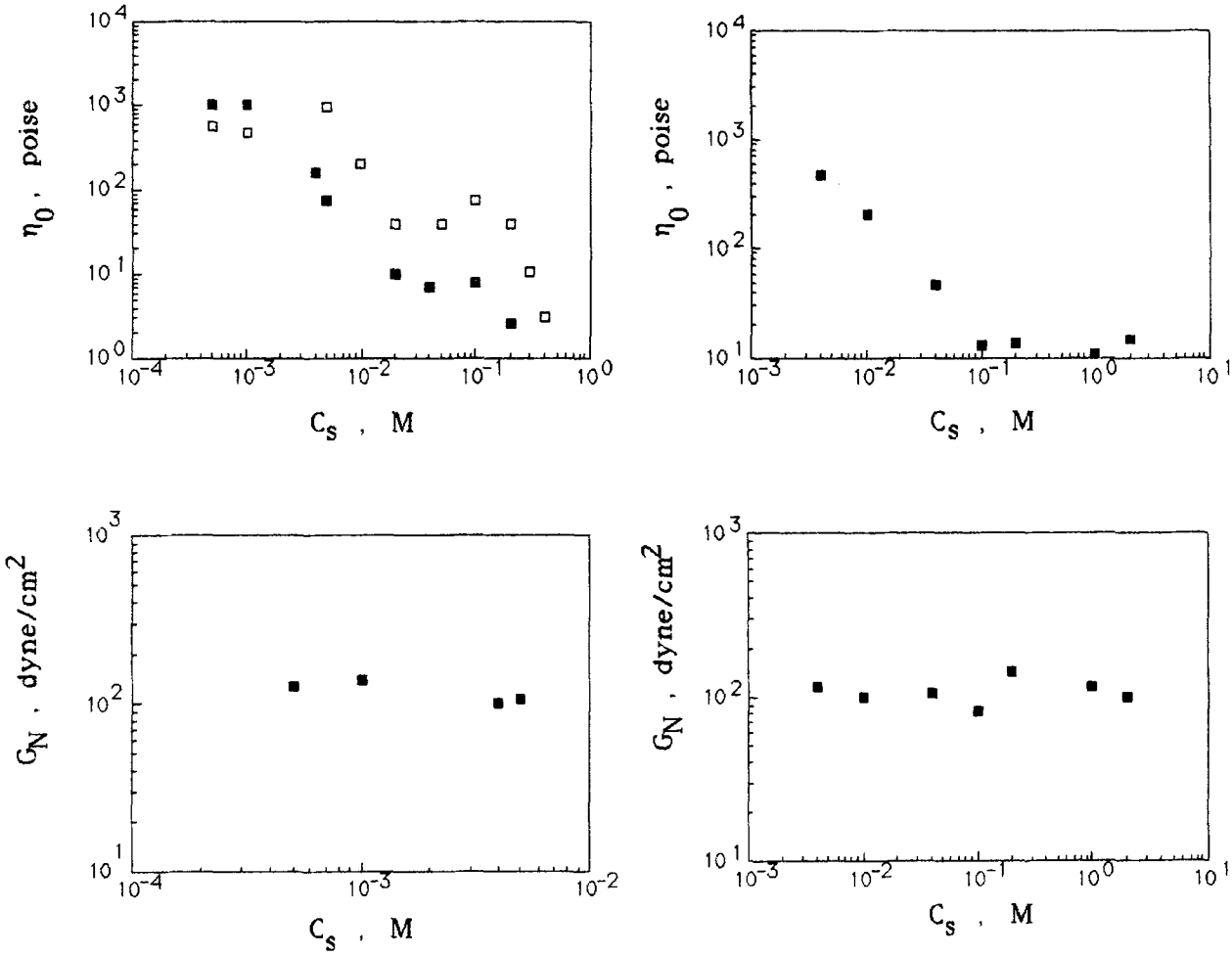

Fig. 7. The salt-concentration dependence of the η_0 and G_N values for aqueous salt solutions of C_nTASal at 25 °C. ■) $C_{14}TASal$ of 1.6×10^{-2} g cm^{-3}; □) $C_{16}TASal$ of 10^{-2} g cm^{-3}. Left, in NaSal; right, in NaBr.

slope in a log G'' vs log ω plot was unity for solutions with a slope 2.0 in a log G' vs log ω plot, while that was less than unity for solutions with a gentle slope in a log G' vs log ω plot.

Discussion

Three types of viscoelasticity

Three types of viscoelasticity were observed in aqueous solutions of C_nTASal. The G' and G'' values in the gel-like viscoelasticity were independent of angular frequency; the $|\eta^*|$ values decreased almost linearly with frequency in a double logarithmic plot. In the Maxwell-like viscoelasticity, the G' values increased at lower frequencies and reached the plateau at higher frequencies, while the G'' values had a maximum. The $|\eta^*|$ values were maintained constant at lower frequencies and decreased at higher frequencies. Both G' and G'' values increased monotonously in the polymer-like viscoelasticity, whereas the $|\eta^*|$ values were almost independent of the frequency. The Maxwell-like and polymer-like viscoelasticities were also reported for aqueous NaSal solutions of $C_{16}TAB$ [10]. The types of viscoelasticity which were observed in aqueous solutions of $C_{14}TASal$ are listed in Table 1. The types of spinnability [14] are also included there with the structures of micelles examined by the light-scattering measurement [16].

The aqueous solutions of $C_{14}TASal$ without salt presented the gel-like viscoelasticity at 10.0 $\times 10^{-2}$ g cm^{-3}, while the viscoelasticity of

Table 1. Rheological Characteristics of Aqueous Solutions of $C_{14}TASal$ at 25 °C.

Solvent	C_s, M	c, 10^{-2} g cm^{-3}	Type of viscoelasticity	Type of spinnability[a])	Structure of micelles[b])
Water	0	0.8–3.2	Maxwell + gel	D	linked short rodlike
	0	10.0	gel	C	
NaBr	0.004–0.04	1.6	Maxwell	D	
	0.1–0.2	1.6	polymer	D	
	1–2	1.6		D	
NaSal	0.001–0.004	1.6	Maxwell	D	
	0.02–0.2	1.6	polymer	D	entangled rodlike
	> 0.3	1.6		no	small

[a])from [14].
[b])from [16].

the solutions below 3.2×10^{-2} g cm^{-3} belonged to the Maxwell-type, which included the contribution of the gel-like viscoelasticity. The solutions revealed a type-C spinnability at surfactant concentrations above 3.5×10^{-2} g cm^{-3} and a type D spinnability at $(1 - 3.5) \times 10^{-2}$ g cm^{-3} [14]. In the light-scattering experiment [16], the external interference effect indicating a strong intermicellar correlation was apparent above 0.1×10^{-2} g cm^{-3} and the effect weakened with decreasing the surfactant concentration, while very short rodlike micelles were formed in the aqueous solutions.

In aqueous solutions of C_nTASal without salt, the three-dimensional pseudo-network may be formed over long distances by the pseudo-linkages between short rodlike micelles, which are broken by the applied shear and result in the shear-thinning viscosity. At high surfactant concentrations where the intermicellar attractive interaction is strong, the pseudo-linkages are abundant, and the solutions behave like gels. Then the viscoelasticity has a long life-time, the stress is not released immediately, and the storage and loss moduli are scarcely changed by the sinusoidal stress, suggesting a strong elastic response. Therefore, the solutions present the type-C spinnability which is characteristic of the more elastic solutions.

The linkages loosen as the surfactant concentration decreases, because the intermicellar interaction decreases. Since the elastic response weakens, the spinnability changes from elastic to viscous behavior, i.e., from type C to D. The stress is released readily and, therefore, the η_0 and G_N values decrease with a decrease in surfactant concentration. Simultaneously, the gel-like viscoelasticity varies partly to Maxwell-type for which the relaxation is concentrated to a certain time. The relaxation in Maxwell-type viscoelasticity might correspond to the variation of network structure due to the break and reformation of pseudo-linkages.

The thermoreversible hydrogen bonding interaction between the functional residues on a polymer chain gave rise to the formation of a thermoplastic elastomeric network [21, 22]. As the intermolecular hydrogen bond linkages multiply, the viscoelastic characteristic of the elastomers was affected, especially, at low frequency or long time region, and the viscoelasticity varied from polymer-type to gel-type. The pseudo-linkages between rodlike C_nTASal micelles may be participated by the salicylate ions directly or through hydrated waters. Then, the aqueous solutions of C_nTASal may behave like thermoplastic elastomers.

The external interference effect between C_nTASal micelles diminished with the addition of NaSal and was imperceptible above 0.001 M NaSal [15, 16], suggesting the partial break of pseudo-linkages. Simultaneously, the length of rodlike $C_{14}TASal$ micelles increased from 13 nm in water to 1300 nm in 0.1 M NaSal at 25 °C [16]. The type-D spinnability which was observed in aqueous solutions of $C_{14}TASal$ at 25 °C exhibited a sharp maximum at NaBr concentration below 0.04 M and a shallow minimum around 0.7 M NaBr [14]. A corresponding maximum in aqueous NaSal solutions was reached at NaSal concentrations below 0.02 M. However, the viscoelasticity varied from

the Maxwell + gel-type to the polymer-type through the Maxwell-type with an addition of NaBr or NaSal.

The addition of salt shields electrostatic repulsion between micelles and induces the growth and entanglement of rodlike micelles [15, 16]. Moreover, the interaction between micelle and water is weakened by the salting-out effect, and the pseudo-linkages between C_nTASal micelles through salicylate ions are broken partially. On addition of a small amount of salt, the micellar growth overcomes the destruction of pseudo-linkages, and the opposite occurs on further addition of salt. The inversion of the compensation of effects may occur at the maximum of the spinnability, at the larger maximum of η_0, and at the longer value of the relaxation time.

After such inversion, i.e., above ~ 0.001 M salt, the Maxwell-type viscoelasticity is dominant because the contribution of gel-type viscoelasticity disappears. However, as the pseudo-linkages are broken further and the micelles grow more at higher salt concentrations, the viscoelasticity of aqueous salt solutions of C_{14}TASal changes to polymer-like. Since the polymer-like viscoelasticity was observed in solutions at salt concentrations above 0.02 M where long rodlike micelles were formed and entangled [16], the initial linear increase of G' and G'' against ω in double logarithmic plots corresponds to the flow (terminal) region on the viscoelasticity of entangled polymers in semi-dilute or concentrated solutions, but not to the Rouse chains in dilute solutions [19]. The initial slopes for G' and G'' were 2 and 1, respectively, as expected. The increase in η_0 from 0.04 M to 0.1 M is due to the promotion of entanglement.

The effect of counterion species

Bromide ions bind electrostatically on a micelle surface and play a part to lengthen rodlike micelles, even at high NaBr concentrations. On the other hand, salicylate ions penetrate into a micelle [23]. Such specific binding caused, besides the growth of rodlike micelles, the inversion of the net surface charge of C_nTASal micelles from positive to negative with the addition of 0.1 M NaSal [15]. Above 0.1 M NaSal where excess salicylate ions penetrate into a micelle and the net charge of micelles is negative, the electrostatic repulsion occurs on the micelle surface and the occupied area of a head group increases. Then, the rodlike shape of micelles cannot be maintained any more and the size of micelles becomes as small as spherical ones [15, 16]. Therefore, the intermicellar interaction such as the entanglement disappears.

The difference of salt effect between NaBr and NaSal is also remarkable on the rheological properties. The spinnability was maintained even at 2 M NaBr, whereas it disappeared above 0.3 M NaSal at 25 °C [14]. The η_0 values of aqueous NaBr solutions were constant at high NaBr concentrations, but those of aqueous NaSal solutions decreased after a small maximum at 0.1 M NaSal.

The salt effect on the rheological behavior of aqueous solutions of C_nTASal micelles is apparent, when the results by Shikata et al. [10] are compared with those in this paper. They prepared micellar solutions by adding NaSal to aqueous solutions of C_{16}TAB. In such a situation, bromide ions coexist at equimolar amount with surfactant ions and act differently with salicylate ions. Especially, the effect of bromide ions was dominant at NaSal/C_{16}TAB molar ratio lower than unity, where polymer-like viscoelastic behavior was observed, but the gel-like viscoelasticity was not. As the NaSal/C_{16}TAB ratio increases near unity, salicylate ions become effective and the Maxwell-type viscoelasticity was obtained. This molar ratio is comparable to that at which the Maxwell-type viscoelasticity was observed in this work.

Relation between viscoelasticity and spinnability

Figure 8 shows the plot of spinnability as a function of τ^2/η_0 for aqueous salt solutions of C_{14}TASal at 25 °C, where τ is the relaxation time. $\Delta L_0/\Delta v$ is the ratio of the intrinsic drawing length to the drawing velocity in the type-D spinnability and the numerical values were taken from the literature [14]. The $\Delta L_0/\Delta v$ values which are equivalent to the spinning time have a relation of

$$\Delta L_0/\Delta v \sim \tau^2/\eta_0 \,. \qquad (1)$$

This means that the spinnability depends on the dynamic relaxation of a solution, as suggested by Nakagawa [24], who concluded that the relaxation time was comparable with the spinning time.

Many investigations of uniaxial elongation [17, 25–36] have been reported in connection with the spinning process of the fiber. When the Maxwell

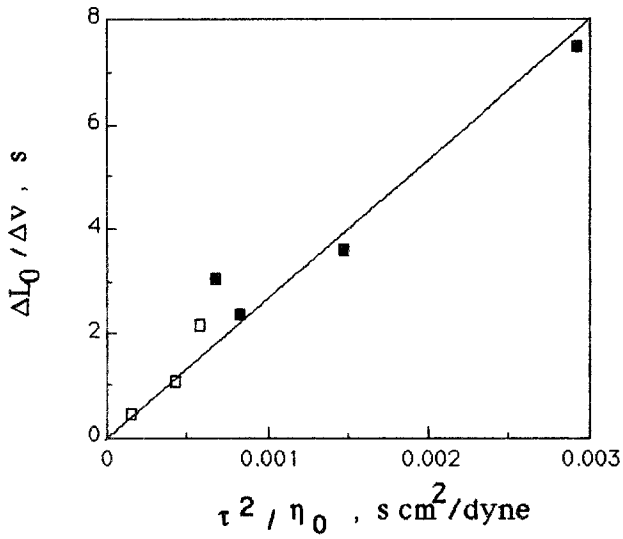

Fig. 8. The plot of spinnability as a function of τ^2/η_0 for aqueous salt solutions of $C_{14}TASal$ at 25 °C. □) in NaSal; ■) in NaBr

liquid is elongated at a constant velocity, the deformation rate decreases with time t, and the stress σ at the limit of long time is described by

$$\sigma \sim (Bt + C)\exp(-t/\tau) , \qquad (2)$$

where B and C are constants [29]. It can be recognized that the stress exhibits a maximum at the relaxation time τ. The maximum stress is reached after long times for the solutions with long relaxation time. In the solutions of type-D spinnability, the elongated thread is broken at the maximum stress, and the spinnability strengthens as the magnitude of the maximum stress lowers, if it is proportional to the elastic modulus.

Suppose that the tension is uniform over the whole thread. When the deformation rate is perturbed at a local part of a thread and the thread thins locally, the stress at the same part increases. If, at the beginning of the elongation ($t \ll \tau$), the whole deformation rate of the thread is fast, the local increase of the deformation rate by the local increase of the stress is negligibly small and the perturbation of the deformation rate or of the thread diameter is readily relieved. This aspect belongs to the time region where the stress increases in Eq. (2).

After being elongated for long times ($t \sim \tau$), the whole deformation rate of the thread decreases, but the local deformation rate increases in proportion to the local increase of the stress by the perturbation. When the latter is superior to the former, the thread diameter becomes thinner. This behavior occurs at the time where the stress is maximum.

When $L_{0,c}$ represents the intrinsic drawing length at high velocity or the constant value of intrinsic drawing length in the type C spinnability, the $L_{0,c}$ values decreased with increasing surfactant concentration [14]. On the other hand, an increase in surfactant concentration caused the increase in G_N values. In the type-C spinnability where the elastic modulus is very strong, the maximum value of the stress is so high that the stress by the elongation is larger than the cohesion force of the thread and the thread is pulled back elastically into the solution reservoir. The elastic pulling-back strengthens with an increase in G_N and the $L_{0,c}$ values shorten.

References

1. Imae T (1989) Langmuir 5:205
2. Sasaki M, Imae T, Ikeda S (1989) Langmuir 5:211
3. Ulmius J, Wennerström H, Johansson LB-Å, Lindblom G, Gravsholt S (1979) J Phys Chem 83:2232
4. Hoffmann H, Platz G, Rehage H, Schorr W (1981) Ber Bunsenges Phys Chem 85:877
5. Hoffmann H, Platz G, Rehage H, Schorr W (1982) Adv Colloid Inter Sci 17:275
6. Rehage H, Hoffmann H (1983) Faraday Discuss Chem Soc 76:363
7. Angel M, Hoffmann H, Löbl M, Reizlein K, Thurn H, Wunderlich I (1984) Progr Colloid Polym Sci 69:12
8. Thurn H, Löbl M, Hoffmann H (1985) J Phys Chem 89:517
9. Hoffmann H, Löbl H, Rehage H, Wunderlich I (1985) Tenside Deterg 22:290
10. Shikata T, Hirata H, Kotaka T (1987) Langmuir 3:1081; (1988) Langmuir 4:354; (1989) Langmuir 5:398
11. Rehage H, Hoffmann H (1988) J Phys Chem 92:4712
12. Shikata T, Hirata H, Takatori E, Osaki K (1988) J Non-Newtonian Fluid Mechanics 28:171
13. Gravsholt S (1976) J Colloid Interface Sci 57:575
14. Imae T, Hashimoto K, Ikeda S (1990) Colloid Polym Sci 268:460
15. Imae T (1990) J Phys Chem 94:5954
16. Imae T, submitting
17. Ide Y, White JL (1976) J Appl Polym Sci 20:2511
18. Okuda H, Imae T, Ikeda S (1987) Colloids Surfaces 27:187
19. Lodge AS (1964) Elastic Liquids; Academic Press: New York; Ferry JD (1980) Viscoelastic Properties of Polymers; 3rd ed, Wiley: New York
20. Cox WP, Merz EH (1958) J Polym Sci 28:619
21. Stadler R, de Lucca Freitas L (1986) Colloid Polym Sci 264:773
22. de Lucca Freitas L, Stadler R (1987) Macromolecules 20:2478

23. Olsson U, Söderman O, Guéring P (1986) J Phys Chem 90:5223
24. Nakagawa T (1952) Bull Chem Soc Japan 25:88; 25:93
25. Denn MM, Marrucci G (1971) AIChE J 17:101
26. Everage Jr AE, Gordon RJ (1971) AIChE J 17:1257
27. Denn MM, Petrie CJS, Avenas P (1975) AIChE J 21:791
28. Kamei E, Onogi S (1976) Polymer J 8:347
29. Fisher RJ, Denn MM (1976) AIChE J 22:236
30. Denn MM, Marrucci G (1977) J Non-Newtonian Fluid Mech 2:159
31. Petrie CJS (1977) J Non-Newtonian Fluid Mech 2:221
32. Ide Y, White JL (1977) J Non-Newtonian Fluid Mech 2:281
33. Ide Y, White JL (1978) J Appl Polym Sci 22:1061
34. Gupta RK, Puszynski J, Sridhar T (1986) J Non-Newtonian Fluid Mech 21:99; 21:115.
35. Sridhar T, Gupta RK (1988) J Non-Newtonian Fluid Mech 27:349
36. Chan RC, Gupta RK, Sridhar T (1988) J Non-Newtonian Fluid Mech 30:267

Received January 24, 1991;
accepted June 6, 1991

Authors' address:

Toyoko Imae
Department of Chemistry
Faculty of Science
Nagoya University
Chikusa
Nagoya 464, Japan